

Coding Schemes for the Noisy Torn Paper Channel

Frederik Walter*, Maria Abu-Sini*, Nils Weinhardt, Antonia Wachter-Zeh

School of Computation, Information and Technology, Technical University of Munich, DE-80333 Munich, Germany

Emails: {frederik.walter, maria.abu-sini, nils.weinhardt, antonia.wachter-zeh}@tum.de

Abstract—To make DNA a suitable medium for archival data storage, it is essential to consider the decay process of the strands observed in DNA storage systems. This paper studies the decay process as a probabilistic noisy torn paper channel (TPC), which first corrupts the bits of the transmitted sequence in a probabilistic manner by substitutions, then breaks the sequence into a set of noisy unordered substrings. The present work devises coding schemes for the noisy TPC by embedding markers in the transmitted sequence. We investigate the use of static markers and markers connected to the data in the form of hash functions. These two tools have also been recently exploited to tackle the noiseless TPC. Simulations show that static markers excel at higher substitution probabilities, while data-dependent markers are superior at lower noise levels. Both approaches achieve reconstruction rates exceeding 99% with no false decodings observed, primarily limited by computational resources.

I. INTRODUCTION

DNA strands used for data storage tend to decay over time, causing strands to break into short fragments [8]. Moreover, DNA synthesis and sequencing processes are error-prone, introducing insertions, deletions, and substitutions. Consequently, enabling long-term storage in such systems necessitates algorithms capable of recovering data from a set of disordered, noisy substrings.

The probabilistic binary noisy torn paper channel (TPC) models this decay and noise accumulation. This channel takes a binary sequence, corrupts its bits uniformly at random with a substitution probability p_s , and subsequently breaks the noisy sequence at any position with probability $p_b = \frac{\alpha}{\log_2 n}$, where n denotes the length of the transmitted sequence. The capacity of this channel has been investigated in [22]. This paper devises coding schemes for the noisy TPC that enable the reconstruction of the transmitted sequence from the received set of unordered noisy fragments. These schemes provide valuable insights and potential solutions for addressing the decay challenges inherent in DNA storage systems.

This paper presents two coding schemes for the noisy TPC. As a first step, we focus on the case of breakage and substitutions solely, and hence leave the investigation of insertions and deletions for future work. The two devised schemes build upon existing work [11], [27].

A standard approach to reconstructing a sequence from unordered fragments involves interleaving a codeword of an era-

sure code with a marker followed by an index. The marker facilitates index detection, which subsequently identifies the fragment's location. This technique is inspired by the *interleaving pilot scheme* proposed in [27]. However, a significant drawback of this scheme, as illustrated in Fig. 3, is that the interleaved indices are independent of the data. Breakages occurring between indices yield fragments devoid of position information, leading to ambiguity in their placement. This results in multiple fragment permutations that appear equally valid. To mitigate this ambiguity, [11], [18] proposed interleaving the codeword with sequence-dependent information rather than fixed markers. Specifically, [11] suggested interleaving the sequence with hash values derived from data blocks. Thus, the literature primarily employs two tools: (1) interleaving with markers and indices, and (2) interleaving with data-dependent hash values.

A. Our Contribution

In this work, we propose two coding schemes that leverage these tools to address the noisy TPC. The first scheme, detailed in Section II, relies primarily on explicit indexing. It interleaves the sequence with markers (specifically 001), followed by bits from a de Bruijn sequence acting as indices, and parity bits derived from the preceding data block. These parity bits serve to link the data with the structural redundancy.

The second scheme (Section III) adopts a hash-based approach without explicit indices. It interleaves the sequence with hash values designed to be robust against substitutions. While the hash functions, as used in [11], are effective for the noiseless TPC, they are unsuitable here; a single substitution can drastically alter the hash value (the avalanche effect), making it impossible to verify the adjacency of two fragments. To overcome this, we employ locality-sensitive hashing (LSH). LSH ensures that small changes in the data, such as those caused by substitutions, result in minimal changes to the hash value, thereby facilitating the correct identification of consecutive fragments even in the presence of noise.

To correct the substitutions after reconstructing the sequence, both schemes utilize an outer low-density parity-check (LDPC) code. The overall processing pipeline can be seen in Fig. 1.

Finally, Section IV presents simulations evaluating these schemes. We compare the robustness of static markers against data-dependent hashing to maintain reconstruction integrity and identify the optimal operating regimes for each approach.

* These authors contributed equally. Funded by the European Union (Di-DAX, 101115134). Views and opinions expressed are however those of the author(s) only and do not necessarily reflect those of the European Union or the European Research Council Executive Agency. Neither the European Union nor the granting authority can be held responsible for them.

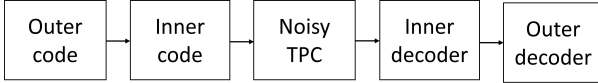


Fig. 1: Concatenated coding scheme for the noisy TPC.

B. Further Related Work

Beyond the discussed approaches, we highlight that [18] and [19] introduced a coding scheme for the noiseless TPC utilizing Varshamov-Tenengolts (VT) codes as hash functions. Furthermore, Ravi et al. studied in [20] and [22] the capacity of the torn paper channel when fragments might be lost with certain probability that depends on their lengths. In parallel, adversarial settings of the TPC have been extensively studied [1], [3], [12], [13], [28]–[33]. These works typically impose constraints such as minimum fragment lengths or upper bounds on the number of breakages and errors. Finally, related models including shotgun sequencing and chop-and-shuffle channels have received significant attention in the recent literature [2], [4], [6], [7], [9], [14]–[17], [21], [24]–[26].

C. Notations

Throughout this paper, we use 1-based indexing. For a sequence \mathbf{x} , the notation $\mathbf{x}_{[i,j]}$ represents the substring starting at index i and ending at index j and $|\mathbf{x}|$ denotes the length. We denote by \mathbf{x}_j^i i repetitions of the j -th bit of sequence \mathbf{x} . The operator $\mathbf{x}_1 \parallel \mathbf{x}_2$ denotes the concatenation of sequences $\mathbf{x}_1, \mathbf{x}_2$. Finally, an *assembly* refers to the method of affixing fragments, at specific positions, as illustrated in Fig. 2. We denote an assembly by small bold letters, and we call an assembly *complete* if it covers the whole codeword. Otherwise, it is referred to as a *partial assembly*.

II. MARKER-BASED CODES WITH INDICES

To tackle the noisy torn paper channel, we propose in this section a concatenated coding scheme as depicted in Fig. 1. Subsection II-A first presents the structure of the codewords, then Subsection II-B elaborates on the reconstruction algorithm. The scheme has several parameters that control its redundancy, failure rate, and decoding run-time complexity. These parameters are d, d', c_1, c_2 , and k , and their role will be explained in the remainder of the section.

A. Encoding algorithm

The outer code used in this scheme is an LDPC code that can correct substitutions. The inner code then interleaves markers and indices in an LDPC codeword. Namely, let \mathbf{x} be a message we aim to transmit, and denote by \mathbf{x}' an LDPC codeword obtained from encoding \mathbf{x} . Furthermore, let \mathbf{r} be a fixed random word. We denote by $\mathbf{x}'' \triangleq \mathbf{x}' + \mathbf{r}$, where the summation is taken over the binary field. The importance of this summation will be explained at the end of the section.

The overall codeword is denoted as $f(\mathbf{x})$, and is constructed from the concatenation of $\frac{|\mathbf{x}''|}{d}$ sequences, which we will refer

to as *encoded blocks*. That is, $f(\mathbf{x}) \triangleq \mathbf{b}_1 \parallel \mathbf{b}_2 \parallel \cdots \parallel \mathbf{b}_{\frac{|\mathbf{x}''|}{d}}$, and the blocks \mathbf{b}_i 's are defined by

$$\mathbf{b}_i \triangleq \mathbf{x}_{[(i-1)d+1,id]}'' \parallel 001\mathbf{m}_i^{c_1} \mathbf{p}_{i,1} \cdots \mathbf{p}_{i,c_2},$$

where

- $\mathbf{m} = \mathbf{m}_1 \cdots \mathbf{m}_{\frac{|\mathbf{x}''|}{d}}$ is a prefix of a shortest de Bruijn sequence that is still longer than $\frac{|\mathbf{x}''|}{d}$, and
- $\mathbf{p}_{i,j}$ is the parity of $\frac{d}{d'}$ bits in $\mathbf{x}_{[(i-1)d+1,id]}''$, specifically of the bits $\mathbf{x}_{(i-1)d+j}''$, $\mathbf{x}_{(i-1)d+j+d'}''$, \dots , $\mathbf{x}_{d-d'+j}''$, which are located at regular intervals of distance d' .

For simplicity we choose parameters d and d' such that d divides $|\mathbf{x}''|$ and d' divides d . In summary, each encoded block \mathbf{b}_i is obtained from concatenating the length- d substring $\mathbf{x}_{[(i-1)d+1,id]}''$, a marker 001, c_1 repetitions of the i -th bit of a de Bruijn sequence \mathbf{m} , and lastly parity bits on the substring $\mathbf{x}_{[(i-1)d+1,id]}''$. As an example, the structure of the overall codeword is illustrated in Fig. 2 when the scheme's parameters are $|\mathbf{x}''| = 12$, $c_1 = 2$, $c_2 = 2$, and $d' = 3$. Specifically, a parity bit $\mathbf{p}_{i,j}$ and its corresponding bits in \mathbf{x}'' are highlighted in the same color in Fig. 2.

As later demonstrated in Subsection II-B, the key idea behind this coding scheme is using the de Bruijn bits as indices to determine the locations of long fragments. To enable correct detection of these indices in a fragment (even in the presence of substitution errors) we do not insert \mathbf{m}_i solely, but a repetition $\mathbf{m}_i^{c_1}$ preceded by the marker 001. This protects the indices from substitutions, and hence extends the interleaving pilot scheme proposed by Shomorony et al. [27] to the noisy TPC as well. The parity bits $\mathbf{p}_{i,j}$'s connect the redundancy with the preceding substring $\mathbf{x}_{[(i-1)d,id]}''$, and hence resolve the challenge exhibited in Fig. 3. Another approach to connect the redundancy with the data is to use hash functions, as proposed in Section III.

Lastly, the significance of adding the random word \mathbf{r} is to reduce the occurrences of the marker 001 in \mathbf{x}'' , and hence enable correct detection of the markers in the noisy fragments.

B. Decoding Algorithm

To explain the decoding algorithm, notice first that the markers, indices, and parities behave like constraints on the codeword. The simplest possible decoding algorithm is one that iterates over all possible permutations of the fragments, and checks how many constraints each permutation violates. A constraint is violated if for instance where we expect a marker 001, we have another substring such as 011, or when a bit $\mathbf{p}_{i,j}$ does not equal the parity of the corresponding bits in $\mathbf{x}_{[(i-1)d+1,id]}''$. The permutation with the fewest violated constraints is most likely to be the correct one. Therefore, we define the *violations count* of an assembly to be the number of constraints (imposed by markers, indices, and parities) it violates. For instance, the violations count of assembly **a** depicted in Fig. 2 equals 4 due to the violations at indices 9, 21, 23, and 26.

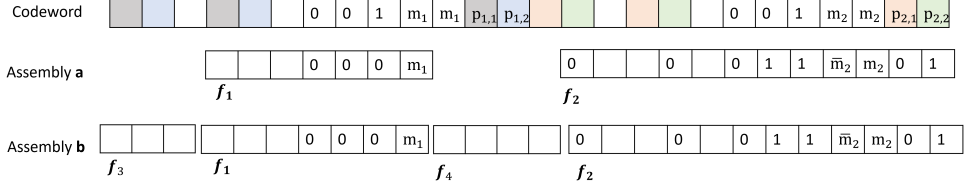


Fig. 2: The structure of the coding scheme presented in Section II is illustrated in the upper word. Markers, followed by indices and parity bits are interleaved into an LDPC codeword. The colors and the values inside the word and the fragments are referred to in Section II. Moreover, affixing the fragments f_1 and f_2 at indices 4 and 15, respectively, constitutes assembly a, which is a partial assembly. Affixing fragments f_3 and f_4 in the gaps results in the complete assembly b.

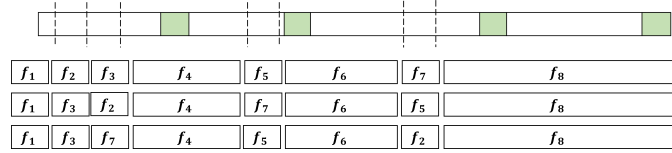


Fig. 3: Markers (that are independent of the data) are highlighted above in green. Breakages between markers resulted in fragments f_2 , f_3 , f_5 , and f_7 . As illustrated all possible permutations of these fragments result in a word that satisfies the markers and the indices constraints. Thus, they are all likely to be the correct permutation of the fragments.

Due to the infeasible run-time complexity of iterating over all permutations, we propose a beam search reconstruction algorithm which operates in the following three phases. Beforehand, denote the input to the decoder, i.e., the received set of t noisy fragments, by $\mathcal{F} = \{f_1, f_2, \dots, f_t\}$.

Phase 1: Define $S_1 \triangleq \{f_i : |f_i| \geq \ell \cdot d_{enc}\}$ to be a set of sufficiently long fragments. The parameter ℓ determines here which fragment's length is considered to be long enough. Since the fragments of S_1 are sufficiently long, they contain multiple markers, and hence a sufficiently long substring of \mathbf{m} that enables detecting their locations. Therefore in Phase 1 we find all possible locations of each fragment $f_i \in S_1$, and accordingly generate assemblies that affix all of the fragments of S_1 . These assemblies are then ranked according to their violations count in an ascending order and the first k are stored in heap A as the initial beams.

Phase 2: In this phase we extend the assemblies in A into complete ones. To that end, we consider each assembly $\mathbf{a} \in A$ and try to extend it by affixing some fragment adjacent to the first attached one in \mathbf{a} . This results in many possible extensions of the assemblies in A . We choose the best k extensions and store them according to their violations count in an ascending order in A . We keep repeating this phase until a sufficient number of complete assemblies is found or until A becomes empty. A becomes empty if at some point we could not extend any partial assembly in it, namely we stored wrong partial assemblies in the previous iterations of Phase 2. Moreover, the parameter k determines the size of the heap A . The larger it is, the more partial assemblies are stored at a time, and hence the higher the run-time complexity of Phase 2 is, but the smaller the failure rate of the decoding algorithm gets.

Phase 3: In Phase 2 we collect a certain number of complete assemblies. Next, in Phase 3 we extract the corrupted bits from the LDPC codeword \mathbf{x}'' and apply 100 iterations

of the min-sum decoding algorithm on these complete assemblies. The output of this phase is a set \mathcal{L} . Whenever the 100 iterations of the min-sum decoder converge to an LDPC codeword, we add it to the set \mathcal{L} . The reconstruction is considered to be successful if at the end \mathcal{L} consists of the single correct message we aimed to transmit. In the simulations we observed that all failures are due to an empty set \mathcal{L} rather than \mathcal{L} consisting of multiple words. That is, even when we applied the min-sum decoder on a wrong assembly, the 100 iterations did not converge to a wrong LDPC codeword. The failure reason we mostly focused on in this work is when A is empty or does not contain the correct assembly.

III. NESTED CODES WITHOUT INDICES

For moderate codeword lengths with few fragments, explicit indices are unnecessary. Instead, we locate the longest fragment using markers and fragment lengths, then employ beam search to concatenate the rest.

A. Encoding Scheme

We adapt the nested reassembly codes of [11] for the noisy TPC. The encoder uses L layers with branching factor m . At layer $\ell = 0$, data is split into m^{L-1} blocks of d bits. A marker $\mathbf{p}_\ell \in \{0, 1\}^{p_\ell}$ follows each block i :

$$\mathbf{c}_i^{(\ell)} = \mathbf{d}_i^{(\ell)} \parallel \mathbf{p}_\ell, \quad (1)$$

where $\mathbf{d}_i^{(\ell)}$ is the data of block i at layer ℓ . Higher layers $\ell > 0$ concatenate m layer- $(\ell - 1)$ codewords to form data blocks:

$$\mathbf{d}_i^{(\ell)} = \mathbf{c}_{mi}^{(\ell-1)} \parallel \mathbf{c}_{mi+1}^{(\ell-1)} \parallel \dots \parallel \mathbf{c}_{mi+m-1}^{(\ell-1)}. \quad (2)$$

The final codeword \mathbf{x} corresponds to layer $L - 1$. No top-level parity is needed as the outer LDPC validates the assembly (see Fig. 4). The nested code rate is

$$R_{\text{Nested}} = \frac{m^{L-1} \cdot d}{\sum_{\ell=0}^{L-1} m^{L-1-\ell} \cdot (m^\ell \cdot d + p_\ell)}, \quad (3)$$

yielding a total rate $R = R_{\text{LDPC}} \cdot R_{\text{Nested}}$.

We replace static markers with Locality-Sensitive Hash (LSH) values, computed as majority votes over data bit subsets. Unlike the hashes with high avalanche effect used in [11], this LSH is robust to small errors. We compare three subset selection schemes (Fig. 5):

- **Block (Block):** Contiguous data blocks.
- **Stride 1 (LSH1):** Bits at regular intervals.

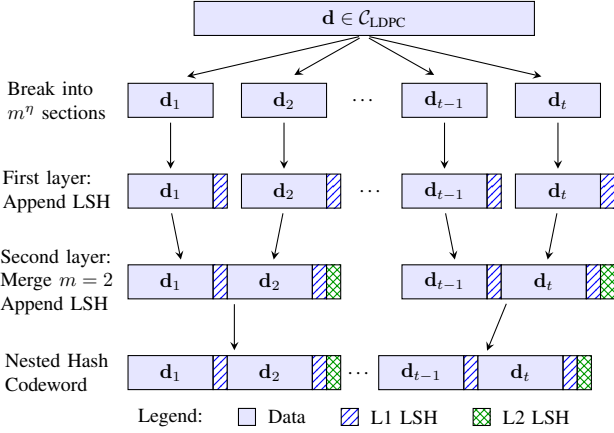


Fig. 4: Nested encoding with $L = 3$ layers and branching factor $m = 2$. Each block contains d data bits and p_ℓ parity bits at layer ℓ .

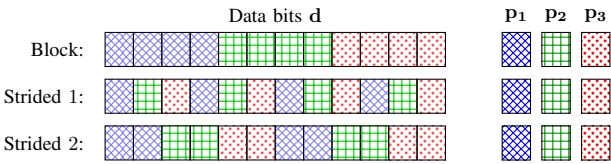


Fig. 5: Subset selection schemes for Locality-Sensitive Hashing (LSH). Each parity bit is derived from a majority vote over the similarly highlighted data bits.

- **Stride 2 (LSH2):** Larger stride to reduce shift sensitivity.

An illustration of the different subset selection schemes for a data block of length $d = 12$ is provided in Fig. 5. A comparison of their performance in the decoding process is presented in Section IV.

B. Nested Hash Decoding

We reconstruct \mathbf{x} from fragments \mathcal{F} using a two-phase beam search.

Phase 1: Beam Initialization. We start with the longest fragment $\mathbf{f}_{\max} \in \mathcal{F}$. Its start position must correspond to the cumulative length of a subset of remaining fragments \mathcal{L} :

$$\mathcal{S} = \left\{ s : s = \sum_{L \in \mathcal{L}} L, \mathcal{I} \subseteq \mathcal{L} \right\}. \quad (4)$$

For each $s \in \mathcal{S}$, we compute the parity distance $\Delta(\mathbf{f}_{\max}, s)$ by comparing recomputed hashes to stored bits. Positions with equal distance are grouped into beams.

Phase 2: Beam Search Assembly. We maintain beams \mathcal{B} , each being a partial assembly with a parity distance. Iteratively, the best beam is expanded by prepending or appending unused fragments, and new distances are computed. We retain the best B_{\max} beams. Upon finding a complete assembly, we apply LDPC belief propagation. If successful, the codeword is returned; otherwise, the search continues.

C. Parameter Selection

The fragment length d is critical. Phase 1 requires a fragment covering at least one layer-0 block to estimate position.

Algorithm 1 Beam Search Fragment Assembly

Require: Fragment set \mathcal{F} , codeword length n , max beams B_{\max}
Ensure: Assembled codeword $\hat{\mathbf{x}}$ or failure

- 1: $f_{\max} \leftarrow$ longest fragment in \mathcal{F}
- 2: $\mathcal{L} \leftarrow$ multiset of lengths in $\mathcal{F} \setminus \{f_{\max}\}$
- 3: $\mathcal{S} \leftarrow \{s : s = \sum_{i \in I} \ell_i, I \subseteq \mathcal{L}\}$ ▷ Subset sums
- 4: **for** each $s \in \mathcal{S}$ **do**
- 5: Compute parity distance $\Delta(f_{\max}, s)$
- 6: Group positions by distance into beams $\mathcal{B} = \{B_1, B_2, \dots\}$
- 7: **while** $\mathcal{B} \neq \emptyset$ **do**
- 8: Pop beam B with lowest parity distance from \mathcal{B}
- 9: **if** B spans full length n **then**
- 10: Decode with LDPC decoder
- 11: **if** valid codeword found **then**
- 12: **return** decoded codeword
- 13: **for** each unused fragment $f_j \in \mathcal{F} \setminus B$ **do**
- 14: **for** $op \in \{\text{prepend, append}\}$ **do**
- 15: $B' \leftarrow$ apply op using f_j on B
- 16: Compute parity distance for all positions in B'
- 17: **if** $|B'| < B_{\max}$ **or** $\Delta(B') < \max_{B_i \in \mathcal{B}} \Delta(B_i)$ **then**
- 18: Add B' to \mathcal{B} (remove worst beam if at capacity)
- 19: **return** failure

In Phase 2, we prefer fragments that complete blocks to verify hashes early. Incomplete blocks delay verification and increase search space, causing failures. Thus, we choose the smallest feasible d .

IV. SIMULATION RESULTS

We evaluate the proposed coding schemes under varying breakage parameters $\alpha \in \{0.05, 0.07, 0.10\}$ and substitution probabilities $p_s \in \{0.4\%, 0.9\%, 1.8\%, 5\%\}$. Efficiency is maintained by using IEEE 802.16e WiMAX and IEEE 802.22 WRAN LDPC codes [10] with adaptive rates and lengths (Table I). Decoding is performed via the product-sum algorithm (50 iterations) for index-free codes [23] and the min-sum algorithm (100 iterations) for index-based codes [5].

p_s	0.4%	0.9%	1.8%	5%
LDPC Rate	0.83	0.75	0.66	0.5
α	0.05	0.07	0.10	
LDPC Length	1152	576	384	

TABLE I: LDPC code rates and lengths for different substitution probabilities and breakage parameters.

Reconstruction relies on a beam search where the number of beams and maximum number of iterations on the beams are adapted to the channel parameters as can be seen in Tables II and III in the appendix. Failures were solely due to resource exhaustion (limited number of beams or search limits on the beams); importantly, no incorrect codewords were returned.

A. Marker Scheme Comparison

We first compare the four marker strategies (Section III) using $n = 1264$ and $\alpha = 0.05$. As shown in Fig. 6, a trade-off exists: static markers are more robust at higher substitution probabilities ($p_s = 1.8\%$), whereas the data-dependent LSH scheme (specifically Stride 2) prevails at lower noise levels ($p_s = 0.9\%$). This suggests that LSH offers better efficiency when data integrity is higher, while static markers provide necessary anchors in noisier conditions.

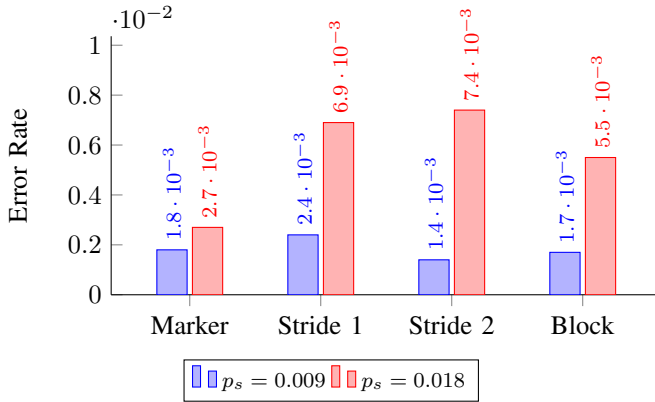


Fig. 6: Comparison of frame error rates (FER) across different marker schemes.

B. Achievable Rates

Our schemes successfully reconstructed codewords with probability $> 99\%$ in all tested scenarios. Figures 7 and 8 display the achievable rates against theoretical capacity [22]. Relaxing search constraints consistently allows the algorithm to recover failed codewords, indicating that the limitation in the recovery rates lies in search complexity rather than code construction.

We tested both coding schemes for $\alpha = 0.05$ and $p_s \in \{0.004, 0.009, 0.018, 0.05\}$, and for these settings we sought sets of the schemes' parameters that maximize the code rate while still ensuring reconstruction probability $> 99\%$ and acceptable decoding run-time complexity. The obtained code rates are depicted in Fig. 7.

The nested coding scheme without indices was also tested for $\alpha \in \{0.05, 0.07, 0.1\}$ and $p_s \in \{0.004, 0.009\}$. The code rates achieving a reconstruction probability of $> 99\%$ are depicted in Fig. 8.

The detailed parameter settings for all simulations conducted can be found in Tables II and III in the appendix.

V. CONCLUSION

In this work, we presented coding schemes for the noisy torn paper channel that simultaneously address fragment reassembly and error correction. Our analysis indicates that in noisy environments, reassembly becomes primarily a computational challenge. Notably, our decoder produced no incorrect codewords; failures resulted solely from timeouts or search

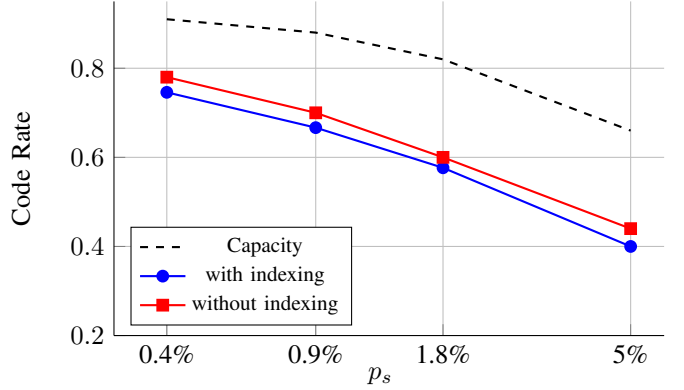


Fig. 7: Code rate vs. p_s for $\alpha = 0.05$ in marker codes with and without indexing.

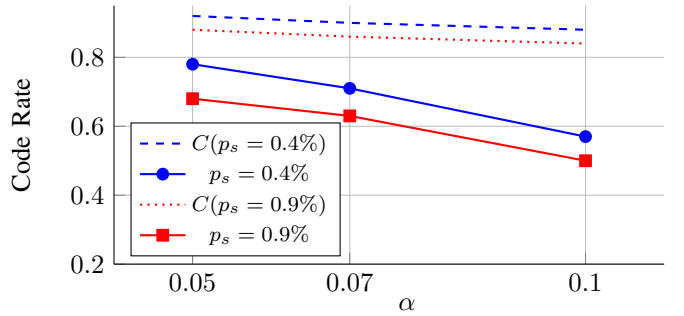


Fig. 8: Code rate vs. α for different substitution error probabilities in marker codes without indexing.

space limits, suggesting that high reliability is attainable with adequate computational resources.

We demonstrated that Locality-Sensitive Hashing (LSH) is a robust tool for reassembly under substitution errors. By tolerating small Hamming distances, LSH preserves fragment connectivity where hashes with high avalanche effect would fail. Additionally, for lower fragmentation rates (small α), combining explicit indices with markers proved effective. The asymptotic analysis of this index-based approach remains an interesting open problem.

Future research directions include optimizing code parameters or integrating static markers with LSH to enhance rates and efficiency. Furthermore, extending the error model to account for insertions and deletions would bring the theoretical framework closer to practical DNA storage conditions. Finally, testing these algorithms on experimental datasets, such as those in [8], is crucial for validating their applicability to long-term data preservation.

REFERENCES

- [1] M. Abu-Sini and R. Heckel, "Near optimal code construction for the adversarial torn paper channel with edit errors," *IEEE International Symposium on Information Theory (ISIT)*, pp. 1–6, Ann Arbor, Michigan, USA, Jun. 2025.
- [2] M. I. Ali, H. Narayanan, and P. Krishnan, "A converse for the capacity of the shotgun sequencing channel with erasures," *arXiv preprint arXiv:2509.21216*, 2025.

- [3] D. Bar-Lev, S. Marcovich, E. Yaakobi, and Y. Yehezkeally, "Adversarial torn-paper codes," *IEEE Transactions on Information Theory*, vol. 69, no. 10, pp. 6414–6427, Oct. 2023.
- [4] G. Bresler, M. Bresler, and D. N. C. Tse, "Optimal assembly for high throughput shotgun sequencing," *BMC Bioinformatics*, vol. 14, no. 5, pp. S18, Jul. 2013.
- [5] A. Cassagne, O. Hartmann, M. Léonardon, K. He, C. Leroux, R. Tajan, O. Aumage, D. Barthou, T. Tonnellier, V. Pignoly, B. Le Gal, and C. Jégo, "AFF3CT: A Fast Forward Error Correction Toolbox!," *SoftwareX*, vol. 10, pp. 100345, 2019.
- [6] R. Gabrys and O. Milenovic, "Unique reconstruction of coded strings from multiset substring spectra," *IEEE Transactions on Information Theory*, vol. 65, no. 12, pp. 7682–7696, Dec. 2019.
- [7] S. Ganguly, E. Mossel, and M. Racz, "Sequence assembly from corrupted shotgun reads," *IEEE International Symposium on Information Theory (ISIT)*, pp. 265–269, Barcelona, Spain, Jul. 2016.
- [8] A. L. Gimpel, W. J. Stark, R. Heckel, and R. N. Grass, "Challenges for error-correction coding in DNA data storage: Photolithographic synthesis and DNA decay," *Digital Discovery*, vol. 3, no. 12, pp. 2497–2508, 2024.
- [9] R. Heckel, I. Shomorony, K. Ramchandran, and D. N. C. Tse, "Fundamental limits of DNA storage systems," *IEEE International Symposium on Information Theory (ISIT)*, pp. 3130–3134, Aachen, Germany, Jun. 2017.
- [10] M. Helmling, S. Scholl, F. Gensheimer, T. Dietz, K. Kraft, O. Griebel, S. Ruzika, and N. Wehn, "Database of channel codes and ML simulation results," *RPTU Rheinland-Pfälzische Technische Universität Kaiserslautern-Landau*, 2025. [Online]. Available: www.rptu.de/channel-codes
- [11] X. Jiao, B. Jiao, J. Mu, and H. Han, "Efficient nested hash reassembly codes for torn paper channels," *IEEE Transactions on Communications*, vol. 73, no. 10, pp. 8607–8622, Oct. 2025.
- [12] J. Liu and N. Raviv, "Single fragment forensic coding from van der corput sets," *IEEE International Symposium on Information Theory (ISIT)*, pp. 1–6, Ann Arbor, Michigan, USA, Jun. 2025.
- [13] J. Liu and N. Raviv, "Single fragment forensic coding from discrepancy theory," *arXiv preprint arXiv:2508.03938*, 2025.
- [14] A. S. Motahari, G. Bresler, and D. N. C. Tse, "Information theory of DNA shotgun sequencing," *IEEE Transactions on Information Theory*, vol. 59, no. 10, pp. 6273–6289, Oct. 2013.
- [15] A. Motahari, K. Ramchandran, D. N. C. Tse, and N. Ma, "Optimal DNA shotgun sequencing: Noisy reads are as good as noiseless reads," *International Symposium on Information Theory (ISIT)*, pp. 1640–1644, Istanbul, Turkey, Jul. 2013.
- [16] H. Narayanan, P. Krishnan, and N. Parekh, "On achievable rates for the shotgun sequencing channel with erasures," *International Symposium on Information Theory (ISIT)*, pp. 1730–1735, Athens, Greece, Jul. 2024.
- [17] H. Narayanan, P. Krishnan, and N. Parekh, "On achievable rates for the shotgun sequencing channel with erasures," *arXiv preprint arXiv:2401.16342*, 2024.
- [18] S. Nassirpour, I. Shomorony, and A. Vahid, "DNA merge-sort: A family of nested Varshamov-Tenengolts reassembly codes for out-of-order media," *IEEE Transactions on Communications*, vol. 72, no. 3, pp. 1303–1317, Mar. 2023.
- [19] S. Nassirpour and A. Vahid, "Embedded codes for reassembling non-overlapping random DNA fragments," *IEEE Transactions on Molecular, Biological and Multi-Scale Communications*, vol. 7, no. 1, pp. 40–50, Mar. 2021.
- [20] A. N. Ravi, A. Vahid, and I. Shomorony, "Capacity of the torn paper channel with lost pieces," *IEEE International Symposium on Information Theory (ISIT)*, pp. 1937–1942, Melbourne, Australia, Jul. 2021.
- [21] A. N. Ravi, A. Vahid, and I. Shomorony, "Coded shotgun sequencing," *IEEE Journal on Selected Areas in Information Theory*, vol. 3, no. 1, pp. 147–159, Mar. 2022.
- [22] A. N. Ravi, A. Vahid, and I. Shomorony, "Recovering a message from an incomplete set of noisy fragments," *arXiv preprint arXiv:2407.05544*, 2024.
- [23] J. Roffe, "LDPC: Python tools for low density parity check codes," *PyPI*, 2022. [Online]. Available: <https://pypi.org/project/ldpc/>
- [24] J. Sima, N. Raviv, and J. Bruck, "On coding over sliced information," *IEEE Transactions on Information Theory*, vol. 67, no. 5, pp. 2793–2807, May 2021.
- [25] I. Shomorony and R. Heckel, "Capacity results for the noisy shuffling channel," *IEEE International Symposium on Information Theory (ISIT)*, pp. 762–766, Paris, France, Jul. 2019.
- [26] I. Shomorony, G. M. Kamath, F. Xia, T. A. Courtade, and D. N. C. Tse, "Partial DNA assembly: A rate-distortion perspective," *IEEE International Symposium on Information Theory (ISIT)*, pp. 1799–1803, Barcelona, Spain, Jul. 2016.
- [27] I. Shomorony and A. Vahid, "Torn-paper coding," *IEEE Transactions on Information Theory*, vol. 67, no. 12, pp. 7904–7913, Dec. 2021.
- [28] C. Wang, J. Sima, and N. Raviv, "Break-resilient codes for forensic 3D fingerprinting," <https://arxiv.org/pdf/2310.03897.pdf>, 2023.
- [29] C. Wang, J. Sima, and N. Raviv, "Break-resilient codes for forensic 3D fingerprinting," *IEEE International Symposium on Information Theory (ISIT)*, pp. 3148–3153, Athens, Greece, Jul. 2024.
- [30] C. Wang, J. Wang, M. Zhou, V. Pham, S. Hao, C. Zhou, N. Zhang, and N. Raviv, "Secure information embedding in forensic 3d fingerprinting," *34th USENIX Security Symposium (USENIX Security 25)*, pp. 1887–1906, 2025.
- [31] H. Wei, M. Schwartz, and G. Ge, "Reconstruction from noisy substrings," *IEEE Transactions on Information Theory*, vol. 70, no. 11, pp. 7757–7776, Nov. 2024.
- [32] Y. Yehezkeally, D. Bar-Lev, S. Marcovich, and E. Yaakobi, "Generalized unique reconstruction from substrings," *IEEE Transactions on Information Theory*, vol. 69, no. 9, pp. 5648–5659, Sept. 2023.
- [33] Y. Yehezkeally, S. Marcovich, and E. Yaakobi, "Multi-strand reconstruction from substrings," *IEEE Information Theory Workshop (ITW)*, pp. 1–6, Kanazawa, Japan, Oct. 2021.

APPENDIX

Table II provides the parameters used while testing the indices-based scheme for certain values of α and p_s . Here we used parameters d, d', c_1, c_2, k , and ℓ that maximize the overall code rate, while ensuring acceptable error rate and decoding run-time complexity. The following points summarize the intuition behind choosing the depicted values of the parameters d, d', c_1, c_2, k , and ℓ .

- The parameters d, c_1 , and c_2 determine the overall code rate. Thus, we aim to keep the ratio $\frac{d}{d_{enc}} = \frac{d}{d+c_1+c_2+3}$ as small as possible; namely, as close as possible to the capacity of the noiseless torn paper channel $e^{-\alpha}$.
- Regarding the parameter d' , ideally we took $p_{i,j}$ to be the parity of just a few (i.e., 3 or 4) bits in the preceding substring $\mathbf{x}'_{[(i-1)d+1, id]}$. Therefore, we choose $d' = \frac{d}{3}$ or $d' = \frac{d}{4}$.
- For the decoding algorithm, the parameter ℓ determines which fragments are seen as long enough, and hence are considered in Phase 1. The smaller ℓ is, the more time and space Phase 1 would require. Thus, we choose ℓ such that a fragment is considered long if it is slightly larger than the average fragment length given by $\frac{\log_2 n}{\alpha}$. This way we ensure that only a few fragments are affixed in Phase 1.
- The larger k , is the smaller the error rate of the reconstruction algorithm, but the larger the run-time complexity becomes. To see that, recall that k determines how many partial assemblies we maintain in Phase 2. If k is quite small, and wrong partial assemblies have lower violations count compared to the correct one, then we might remove the correct partial assembly from A in Phase 2. In such a case, we will not find the correct complete assembly. On the other hand, if k is too larger, then each time we run Phase 2, we will try to extend many partial assemblies, which incurs a high decoding run-time complexity. Therefore, we choose a value of k that ensures acceptable decoding run-time complexity and error rate at the same time.

Another parameter that has been used to control the error rate and run-time complexity of the decoder is k' , provided in Table II. To determine the location of a long fragment f , we search for two subsequences in f that are most likely to be markers. Recall here that substitutions might occur at markers too. Thus, we consider two subsequences rather than just one. Then, we extract the indices following these markers. These indices constitute substrings of \mathbf{m} , and the goal now is to determine where these substrings occur in \mathbf{m} . If a substring is short, then it might occur several times in \mathbf{m} . The parameter k' determines how many occurrences of this substring we take as potential locations of f . Hence, it is chosen according to $\frac{|\mathbf{x}''|}{d}$ and ℓ .

The number of failures in Table II is the number of iterations in which Phase 2 did not find the correct complete assembly. We observed that in one simulation for $\alpha = 0.05$ and $p_s = 0.018$ Phase 2 did not find the correct complete assembly. Thus, we ran the LDPC decoder in Phase 3 over incorrect assemblies, nevertheless, the belief propagation algorithm managed to recover the correct message. A potential explanation for this, is that the incorrect assemblies found transposed very short fragments and hence we then ran the LDPC decoder on a message corrupted by very few substitutions which it could correct. Here we state that even when we provided the LDPC decoder with incorrect assemblies, it never returned an incorrect message, but the iterations of the belief propagation algorithm did not converge into an LDPC codeword.

Lastly, we recall that in Phase 2 we collected several complete assemblies. Namely in Phase 3 we ranked the best 20 complete assemblies found according to their violations count, and then we ran the LDPC decoder on all of them. The average ranking column in Table II is the average ranking of the correct assembly in Phase 3. Mostly, it was ranked first, yet in some simulations it was ranked a bit high. The highest ranking found was 8.

ID	p_s	α	n	d	d'	c_1	c_2	ℓ	k	k'	Rate overall	Rate LDPC	#iter	#failure	#LDPC err	Average ranking	#successful	Success rate	Used in Figure
1	0.004	0.05	1287	64	16	2	2	3.5	2000	11	0.74592	0.83	7411	3	50	1.03415	7358	0.9928	7
2	0.009	0.05	1296	64	16	2	3	3.5	2000	11	0.66666	0.75	8918	6	25	1.02289	8887	0.9965	7
3	0.018	0.05	1332	64	16	3	4	3.5	2000	12	0.57657	0.66	10^4	21	35	1.0234	9945	0.9945	7
4	0.05	0.05	1440	36	12	3	3	4.5	3000	12	0.4	0.5	10^4	44	18	1.024	9938	0.9938	7
5	0.004	0.07	1320	48	16	2	2	3.5	2000	10	0.72727	0.83	10^4	18	44	1.05369	9911	0.9911	
6	0.009	0.07	1344	48	16	2	3	3.5	2000	10	0.64285	0.75	10^4	34	38	1.03341	9928	0.9928	
7	0.018	0.07	1392	48	16	3	4	3.5	2500	11	0.55172	0.66	10^4	68	34	1.03272	9898	0.9898	
8	0.004	0.1	1376	36	12	2	2	3.6	3000	11	0.69767	0.83	2047	24	12	1.16023	2010	0.9824	

TABLE II: Simulation results for indices-based scheme (Section II). Due to the lack of space, we omitted in the table the length of the used LDPC code, especially that it is equal to 1152 in all of these simulations.

ID	p_s	α	n	d_{sec}	Parity	Hash	Rate overall	Rate LDPC	Length LDPC	#Beams	max BS iter timeout	#iter	#time-out	#err LDPC	#successful	Success rate	Used in Figure
1	0.004	0.05	1231	32	[2, 1, 1]	LSH2	0.78	0.83	1152	10^4	10^5	10^4	1	13	9986	0.9986	
2	0.004	0.05	1231	32	[2, 1, 1]	LSH2	0.78	0.83	1152	10^4	10^5	10^4	2	8	9990	0.9990	7, 8
3	0.009	0.05	1231	32	[2, 1, 1]	LSH2	0.70	0.75	1152	10^4	10^5	10^4	5	1	9994	0.9994	7, 8
4	0.009	0.05	1267	32	[3, 1, 1]	LSH2	0.68	0.75	1152	10^4	10^5	10^4	5	1	9994	0.9994	
5	0.009	0.05	1267	32	[3, 1, 1]	LSH2	0.68	0.75	1152	10^4	10^5	10^4	8	1	9991	0.9991	
6	0.009	0.05	1264	18	[1, 3, 0, 0]	Marker	0.68	0.75	1152	10^4	10^5	10^4	18	2	9980	0.9980	6
7	0.009	0.05	1264	18	[1, 3, 0, 0]	LSH1	0.68	0.75	1152	10^4	10^5	10^4	24	2	9974	0.9974	6
8	0.009	0.05	1264	18	[1, 3, 0, 0]	Block	0.68	0.75	1152	10^4	10^5	10^4	17	2	9981	0.9981	6
9	0.009	0.05	1264	18	[1, 3, 0, 0]	LSH2	0.68	0.75	1152	10^4	10^5	10^4	14	2	9984	0.9984	6
10	0.018	0.05	1272	32	[3, 2, 1]	LSH2	0.60	0.66	1152	10^4	10^5	10^4	24	2	9976	0.9976	7
11	0.018	0.05	1301	18	[2, 1, 1, 1]	LSH2	0.59	0.66	1152	10^4	10^5	10^4	5	0	9995	0.9995	
12	0.018	0.05	1264	18	[1, 3, 0, 0]	Marker	0.61	0.66	1152	10^4	10^5	10^4	27	1	9972	0.9972	6
13	0.018	0.05	1264	18	[1, 3, 0, 0]	LSH1	0.61	0.66	1152	10^4	10^5	10^4	69	1	9930	0.9930	6
14	0.018	0.05	1264	18	[1, 3, 0, 0]	Block	0.61	0.66	1152	10^4	10^5	10^4	74	1	9925	0.9925	6
15	0.018	0.05	1264	18	[1, 3, 0, 0]	LSH2	0.61	0.66	1152	10^4	10^5	10^4	55	1	9944	0.9944	6
16	0.05	0.05	1309	32	[4, 2, 1]	LSH2	0.44	0.5	1152	10^4	10^5	10^4	50	2	9948	0.9948	7
17	0.05	0.05	1345	32	[5, 2, 1]	LSH2	0.43	0.5	1152	10^4	10^5	7833	33	2	7798	0.9955	
18	0.004	0.07	1231	32	[2, 1, 1]	LSH2	0.78	0.83	1152	10^4	10^5	10^4	350	10	9640	0.9640	
19	0.004	0.07	1344	18	[3, 0, 0, 0]	Block	0.71	0.83	1152	1.5×10^4	1.5×10^5	10^4	227	12	9711	0.9711	
20	0.004	0.07	800	9	[1, 3, 4, 0, 0, 0]	LSH2	0.60	0.83	576	2×10^4	3×10^5	2000	0	1	1999	0.9995	
21	0.004	0.07	752	9	[0, 3, 5, 0, 0, 0]	LSH2	0.64	0.83	576	2×10^4	2×10^5	2000	0	2	1998	0.9990	
22	0.004	0.07	720	9	[0, 2, 5, 0, 0, 0]	LSH2	0.67	0.83	576	2×10^4	2×10^5	10^4	0	21	9979	0.9979	
23	0.004	0.07	720	9	[0, 1, 4, 0, 0, 0]	LSH2	0.71	0.83	576	2×10^4	2×10^5	10^4	0	17	9983	0.9983	8
24	0.009	0.07	1267	32	[3, 1, 1]	LSH2	0.68	0.75	1152	10^4	10^5	10^4	226	0	9774	0.9774	
25	0.009	0.07	800	9	[1, 3, 4, 0, 0, 0]	LSH2	0.54	0.75	576	2×10^4	3×10^5	2000	0	2	1998	0.9990	
26	0.009	0.07	736	9	[0, 3, 4, 0, 0, 0]	LSH2	0.59	0.75	576	2×10^4	2×10^5	10^4	0	11	9989	0.9989	
27	0.009	0.07	688	9	[1, 0, 3, 0, 0, 0]	LSH2	0.63	0.75	576	2×10^4	2×10^5	10^4	1	9	9990	0.9990	8
28	0.018	0.07	1440	18	[4, 2, 0, 0]	Block	0.53	0.66	1152	1.5×10^4	1.5×10^5	10^4	229	1	9770	0.9770	
29	0.004	0.1	848	9	[2, 3, 3, 0, 0, 0]	Block	0.57	0.83	576	1.5×10^4	1.5×10^5	10^3	4	3	993	0.9930	
30	0.004	0.1	560	6	[1, 2, 3, 0, 0, 0]	LSH2	0.51	0.75	384	2×10^4	3×10^5	10^4	3	3	9994	0.9994	
31	0.004	0.1	560	6	[1, 2, 3, 0, 0, 0]	LSH2	0.57	0.83	384	2×10^4	2×10^5	10^4	7	91	9902	0.9902	8
32	0.009	0.1	848	9	[2, 3, 3, 0, 0, 0]	LSH2	0.51	0.75	576	1.5×10^4	1.5×10^5	1000	12	1	987	0.9870	
33	0.009	0.1	856	18	[3, 8, 7, 0, 0, 0]	Marker	0.50	0.75	576	1.5×10^4	1.5×10^5	2000	54	4	1942	0.9710	
34	0.009	0.1	912	9	[1, 3, 7, 8, 0, 0, 0]	LSH2	0.47	0.75	576	1.5×10^4	1.5×10^5	2000	52	0	1946	0.9730	
35	0.009	0.1	912	9	[3, 4, 0, 0, 0, 0, 0]	Marker	0.48	0.75	576	1.5×10^4	1.5×10^5	2000	85	0	1913	0.9565	
36	0.009	0.1	1072	9	[4, 5, 5, 0, 0, 0, 0]	Marker	0.48	0.75	576	2×10^4	2.5×10^5	2000	68	6	1926	0.9630	
37	0.009	0.1	976	9	[2, 3, 7, 8, 0, 0, 0]	LSH2	0.44	0.75	576	2×10^4	5×10^5	2000	36	2	1962	0.9810	
38	0.009	0.1	784	9	[1, 2, 5, 0, 0, 0, 0]	LSH2	0.55	0.75	576	2×10^4	3×10^5	1000	12	0	988	0.9880	
39	0.009	0.1	576	6	[1, 2, 4, 0, 0, 0, 0]	LSH2	0.50	0.75	384	2×10^4	3×10^5	10^4	12	33	9955	0.9955	8

TABLE III: Simulation results for nested hash codes. No experiment resulted in an incorrect assembly; failures are due to timeouts or LDPC decoding errors. LDPC codes of lengths 1152 and 576 are IEEE 802.16e WiMAX codes. The LDPC code of length 384 is a IEEE 802.22 WRAN code. The main error source are timeouts due to beam search not completing within the allotted number of iterations. These timeout occurred when the number of fragments grew large due to higher values of α . Therefore, shorter code lengths were used with higher α values to keep the number of fragments manageable. The rightmost column indicates which simulation data were used in the figures.